

A hybrid learning agent for episodic learning tasks with unknown target distance

Oliver Sefrin^{1*} and Sabine Wölk¹

¹Institute of Quantum Technologies, German Aerospace Center (DLR),
Wilhelm-Runge-Straße 10, Ulm, 89081, Germany.

*Corresponding author(s). E-mail(s): oliver.sefrin@dlr.de;

Abstract

The “hybrid agent for quantum-accessible reinforcement learning”, as defined in (Hamann and Wölk, 2022), provides a proven quasi-quadratic speedup and is experimentally tested. However, the standard version can only be applied to episodic learning tasks with fixed episode length. In many real-world applications, the information about the necessary number of steps within an episode to reach a defined target is not available in advance and especially before reaching the target for the first time. Furthermore, in such scenarios, classical agents have the advantage of observing at which step they reach the target. Whether the hybrid agent can provide an advantage in such learning scenarios was unknown so far.

In this work, we introduce a hybrid agent with a stochastic episode length selection strategy to alleviate the need for knowledge about the necessary episode length. Through simulations, we test the adapted hybrid agent’s performance versus classical counterparts. We find that the hybrid agent learns faster than corresponding classical learning agents in certain scenarios with unknown target distance and without fixed episode length.

Keywords: Quantum Reinforcement Learning, Amplitude Amplification, Hybrid Algorithm, Navigation Problem

1 Introduction

Reinforcement Learning (RL), the Machine Learning framework related to learning through interaction and experience, has shown tremendous success in recent years, surpassing human capability in Atari games (Mnih et al., 2015) or the board game Go (Silver et al., 2017), amongst many others. One of the main reasons for its success is the ever-growing computational power of classical hardware, which allows the implementation of Deep Learning techniques in RL such as Deep Q-Learning (DQN) (Mnih et al., 2015).

However, many problems and problem classes still prove to be difficult even to modern supercomputers due to their unfavorable scaling with the problem size. Here, quantum computation (Nielsen and Chuang, 2010) with the prospect of polynomial or even exponential advantages in problem complexity has excited researchers across many disciplines and even created new research fields. Among the latter, Quantum Machine Learning (QML) (Biamonte et al., 2017) has emerged with the idea of combining the computational benefits of quantum computation with the proven effectiveness of machine learning

approaches. Given the current state of quantum computing hardware in the so-called noisy intermediate-scale quantum (NISQ) era (Preskill, 2018), research in QML has focused on algorithms of low circuit depth and width, such as variational algorithms (Cerezo et al., 2021), or even so-called quantum-inspired methods such as tensor networks (Biamonte and Bergholm, 2017; Orús, 2014; Bridgeman and Chubb, 2017; Huggins et al., 2019). Whereas these methods have the benefit of being applicable on current quantum devices (or even on classical machines in the case of quantum-inspired ansätze), their actual advantage compared to classical methods remains unclear (Schuld and Killoran, 2022; Cerezo et al., 2024).

An example for a QML algorithm with a provable speedup which is, however, not NISQ-ready, is the so-called “hybrid agent for quantum-accessible reinforcement learning” (Hamann and Wölk, 2022). Here, a learning agent learns to solve a given problem by interacting via a set of actions with a problem environment. Based on amplitude amplification (Grover, 1997; Brassard et al., 2002), a quasi-quadratic speedup in terms of the sample complexity compared to corresponding classical agents was proven for a class of RL environments called *deterministic and strictly episodic (DSE)* environments. These environments are reset to an initial state after a fixed number of interaction steps defining the *episode length*. Further, choosing an action in the current state yields one subsequent state with certainty. The *Gridworld* or maze scenario with a fixed episode length is one example of a DSE environment and serves as a toy model in this work.

While many learning scenarios are indeed episodic, a large subset of these is not strictly episodic. That is, episodes may differ in length because, e.g., their end is coupled to reaching some rewarded target state such that the episode length depends on the brevity of the solution found. The *Gridworld* environment without a fixed episode length is an example for such a learning scenario. In general, the hybrid agent (Hamann and Wölk, 2022) can easily be applied to a deterministic and non-strictly episodic environment by choosing a fixed episode length L after which the episode ends, whether the target was reached or not. Yet, the chosen episode length L has crucial influence on the hardness of the learning problem and the

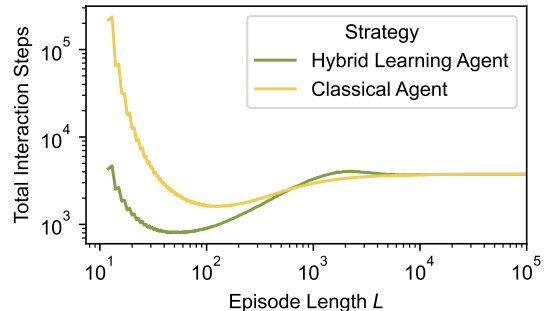


Fig. 1: Comparison of the expected number of total interaction steps performed before finding a defined target for the first time depending on the episode length L . The results stem from a simulation with a *Gridworld* of base size 7×7 and an outer wall distance of 16 (see Section 3.2 for information about the *Gridworld* layouts).

expected total number of interaction steps to learn to solve the problem, both in the classical and the hybrid case. Fig. 1 illustrates this influence. Here, we show the expected number of interaction steps, summed over all episodes, until the defined goal was reached for the first time for a classical and a hybrid agent depending on the fixed episode length L for a given maze example. On the one hand, choosing L small renders the problem hard or even unsolvable for an untrained agent. On the other hand, choosing a large L can lead to a high probability $p_{\text{init}}(L)$ to achieve the defined target within one episode even for an untrained agent. This reduces the number of necessary episodes but makes a large number of interaction steps per episode necessary. For small episode lengths, corresponding to small success probabilities $p_{\text{init}}(L)$, the hybrid agent offers a quasi-quadratic speedup compared to the classical agent. For intermediate episode lengths, the hybrid agent’s quantum overhead results in a slightly worse performance, before it finally converges to the classical agent’s behavior and thus to its performance in the limit of large episode lengths and $p_{\text{init}}(L) \rightarrow 1$. (For a detailed discussion, see Appendix C.)

In summary, the choice of L can have a larger influence on the necessary effort to reach the goal than whether we use a hybrid or a purely classical agent. If enough information about the learning problem were available, an optimal episode length

could be inferred. However, this is usually not the case. Furthermore, a classical learning agent can observe when it reaches the target and then end the episode. In quantum mechanics, observation usually suppresses the effect of interference, which is necessary to gain a quantum advantage. Thus, a predefined episode length is necessary for the hybrid agent. Whether the hybrid agent can outperform classical agents which use the advantage of a flexible episode length and if so, in which scenarios, has not been investigated so far.

In this work, we introduce a hybrid agent with a flexible episode length selection strategy for the case of a deterministic and episodic environment with an unknown target distance. More precisely, we introduce a probabilistic condition which doubles the current episode length when triggered until the target is found for the first time. Reaching the target for the first time is especially challenging while extremely important. Indeed, after having reached the target, the length of the found sequence of actions is obviously sufficient and serves as an upper bound for the optimal episode length. The necessity of reaching the target for the first time efficiently is further underlined by the fact that, at the start of learning, the RL algorithm’s success probabilities are usually the lowest. This indicates that the search for reaching the target for the first time in such a sparse reward environment takes up a significant amount of the total learning time.

By interweaving our probabilistic episode length adaptation with the underlying amplitude amplification algorithm, we manage to solve learning problems without fixed episode length with no additional hyperparameters introduced. We test the extended hybrid agent versus a corresponding classical agent with the same episode length selection strategy and a classical agent with flexible episode length. This latter agent has no fixed episode length and ends an episode only when finding the target. By investigating various layouts of the Gridworld problem, and comparing the performance of the different agents, we can distinguish different learning scenarios where either our hybrid agent or a classical agent with a completely flexible episode length is favorable.

The article is structured as follows: in Section 2, the hybrid agent is introduced in more detail as well as placed in the broader context of

Quantum Reinforcement Learning (QRL). Next, we present the adapted algorithm and explain the simulation methodology in Section 3. In Section 4, we define a new figure of merit tailored to the new problem setting and motivate it before presenting the results. Finally, we provide a conclusion and an outlook in Section 5.

2 Background

2.1 Reinforcement Learning

In RL (Sutton and Barto, 2018), an agent interacts with an environment in a sequence of discrete time steps $t \in \mathbb{N}_0$. The interaction starts with an initial percept, or state, $s_0 \in \mathcal{S}$ from the set of possible percepts \mathcal{S} , which is given to the agent by the environment. At each time step $t \geq 1$, the agent selects an action a_t from the set of possible actions \mathcal{A} based on the previous percept s_{t-1} . This action selection is governed by the agent’s current *policy* $\pi(a|s)$, which is a probability distribution over the set of actions conditional to the current percept. Subsequently, the environment responds with the next percept s_t as well as a real-valued reward r_t . Generally, the response of the environment is probabilistic, with probability distribution

$$\tau(s_t, r_t | s_{t-1}, a_t). \quad (1)$$

Since the probability function only depends on the previous interaction step, it fulfills the Markov property. Hence, this type of RL interaction is a so-called finite *Markov Decision Process* (MDP).

In *deterministic* environments such as Gridworld, eq. (1) is a trivial probability distribution in the sense that it returns unity for one specific combination of percept and reward value (s_t, r_t) and zero for any other combination. To simplify the notation in Algorithm 1, we can thus introduce functions $S : \mathcal{S} \times \mathcal{A} \rightarrow \mathcal{S}$ and $R : \mathcal{S} \times \mathcal{A} \rightarrow \mathbb{R}$ which return the next, deterministic percept s_t and reward r_t , respectively:

$$r_t = R(s_{t-1}, a_t) \quad (2)$$

$$s_t = S(s_{t-1}, a_t) \quad (3)$$

The agent’s task is to adapt its policy such as to maximize the expectation value of the *cumulative*

reward

$$\mathbb{E}_\pi \left[\sum_{t=1}^{\infty} \gamma^t r_t \right], \quad (4)$$

where the subscript π indicates the expectation value upon following policy π . The coefficient $\gamma \in (0, 1]$ is the so-called discount value, which adjusts a trade-off between current and future rewards.

2.2 Hybrid Learning Agent

Our approach builds on the QRL algorithm coined “hybrid agent for quantum-accessible reinforcement learning” (Hamann and Wölk, 2022). This algorithm is embedded in a quantum communication scenario where the RL agent and the DSE environment interact by exchanging quantum states. That is, each action from the set of allowed actions $a \in \mathcal{A}$ is mapped to a quantum state $|a\rangle_A$ and the set of states $\{|a\rangle \mid a \in \mathcal{A}\}$ forms an orthonormal basis. Similarly, the set of percepts $\{s \mid s \in \mathcal{S}\}$ is mapped to orthonormal states $\{|s\rangle_S\}$, and the set of rewards $\{r \mid r \in \mathcal{R}\}$ to orthonormal states $\{|r\rangle_R\}$. Here, the indices A , S , and R indicate the Hilbert spaces for the quantized actions \mathcal{H}_A , percepts \mathcal{H}_S , and rewards \mathcal{H}_R , respectively. We map the initial percept s_0 to

$$|\vec{s}_{\text{init}}\rangle_S = |s_0, \emptyset, \dots, \emptyset\rangle_S \in \mathcal{H}_S^{\otimes(L+1)},$$

with a single-percept default state $|\emptyset\rangle_S \in \mathcal{H}_S$, as the initial quantum state for the sequence of percepts and use $|\vec{0}\rangle_R \in \mathcal{H}_R^{\otimes L}$ as the initial quantum state for the sequence of rewards. Then, in the quantum communication scenario, the response of the environment to the sequence of actions $\vec{a} = (a_1, \dots, a_L)$ within one episode of L interaction steps can be modeled as a unitary U_{env} acting on the multipartite state $|\psi\rangle = |\vec{a}\rangle_A |\vec{s}_{\text{init}}\rangle_S |\vec{0}\rangle_R$ such that

$$U_{\text{env}} |\psi\rangle = |\vec{a}\rangle_A |\vec{s}\rangle_S |\vec{r}\rangle_R.$$

In our RL scenario, we assume a single binary reward r is given at the end of each episode to simplify the learning scenario, such that the reward Hilbert space is two-dimensional.

With α_k ¹ queries of the environment unitary U_{env} , it was shown that an effective phase-kickback oracle

$$O_E |\vec{a}\rangle_A |\vec{s}_{\text{init}}\rangle_S |-\rangle_R = (-1)^{r(\vec{a})} |\vec{a}\rangle_A |\vec{s}_{\text{init}}\rangle_S |-\rangle_R \quad (5)$$

can be realized (Dunjko et al., 2016) when initializing the reward register in the state $|-\rangle_R = \frac{1}{\sqrt{2}}(|0\rangle_R - |1\rangle_R)$. Based on this oracle, a hybrid quantum classical learning agent has been defined in (Saggio et al., 2021; Hamann and Wölk, 2022).

This hybrid learning agent consists of two parts: a quantum part and a classical part. In the quantum part of the hybrid learning agent (Hamann and Wölk, 2022), the agent prepares instead of a single sequence of actions $|\vec{a}\rangle$ a superposition of possible sequence of actions $\sum_{\vec{a}} c_{\vec{a}} |\vec{a}\rangle$ where $|c_{\vec{a}}|^2$ is equal to the probability that the agent chooses the action sequence \vec{a} according to its current policy π . By interacting with the environment, the agent applies a Grover operator on $\sum_{\vec{a}} c_{\vec{a}} |\vec{a}\rangle$ based on the oracle O_E . With this Grover operator, the amplitudes $\{c_{\vec{a}} \mid r(\vec{a}) > 0\}$ of rewarded action sequences can be amplified which enables a quadratic speedup in query complexity (Grover, 1997; Brassard et al., 2002). Following the quantum part of the algorithm, the classical part of the agent starts by measuring the action register. Consecutively, one classical episode with the measured action sequence \vec{a} is performed to determine the corresponding sequence of percepts $\vec{s}(\vec{a})$ and the corresponding reward $r(\vec{a})$ for the measured sequence of actions. This is necessary to infer the actual sequence of percepts encountered by the agent as well as the reward information, since this information was uncomputed in the amplitude amplification procedure to allow for interference. Finally, the policy π of the agent can be updated according to some chosen update rules such as Q-Learning (Watkins and Dayan, 1992) or Projective Simulation (Briegel and De las Cuevas, 2012). Then, the agent proceeds by starting the next quantum part until a predefined ending condition (Hamann and Wölk, 2022) is met.

¹ $\alpha_k = 1$ for basic environments with action-independent percepts s and $\alpha_k = 2$ for environments in which intermediate percepts s are action-dependent (Hamann and Wölk, 2022).

The speedup of the hybrid learning agent has been verified in a proof-of-principle experiment using a nanophotonic processor (Saggio et al., 2021). Likewise, a speedup in decision-making using a quantum walk search approach has been formulated (Paparo et al., 2014) and experimentally verified (Sriarunothai et al., 2018) for a variant of the Projective Simulation algorithm called “Reflecting Projective Simulation” (Briegel and De las Cuevas, 2012). A first extension of the standard RL scenario for the hybrid learning agent concerning changing oracles was investigated in (Hamann et al., 2021).

2.3 Related Work

QRL (Dong et al., 2008), just as Quantum Machine Learning, can be interpreted in many different ways, according to which we aim to structure this overview of related work.

In the broader sense, QRL can be understood as the application of classical RL (Sutton and Barto, 2018) to problems related to quantum computing or quantum technologies. This comprises the usage of RL for quantum circuit optimization (Ostaszewski et al., 2021; Lockwood, 2022; Fösel et al., 2021; Ruiz et al., 2024; Rapp et al., 2024), quantum control (Sivak et al., 2022; Fösel et al., 2018; Bukov et al., 2018; Guatto et al., 2024), or quantum error correction (Nautrup et al., 2019; Sivak et al., 2023).

Another well-established category is QRL with parametrized quantum circuits (PQCs) (Jerbi et al., 2021). Here, PQCs encode the RL agent’s current policy (in policy gradient algorithms such as PPO (Schulman et al., 2017) or DPG/DDPG (Silver et al., 2014; Lillicrap et al., 2019)) or encode an approximate action-value function such as in DQN (Mnih et al., 2015). In a hybrid approach, the PQC’s parameters are updated using a classical feedback loop. Using simulated or real quantum hardware, these methods have been applied to standard Gymnasium (Kwiatkowski et al., 2024) (previously OpenAI Gym (Brockman et al., 2016)) environments such as Cart Pole, Frozen Lake, or Atari Games (Jerbi et al., 2021; Skolik et al., 2022; Chen et al., 2020; Lockwood and Si, 2020, 2021) as well as maze problems (Hohenfeld et al., 2024; Chen et al., 2024).

More recent approaches aim at speeding up the learning process using quantum sub-routines (Ganguly et al., 2023; Zhong et al., 2024), finding better policies with a combined approach of using quantum phase estimation (Kitaev, 1995) and Grover’s search algorithm (Grover, 1997; Wiedemann et al., 2023), or combining quantum computing with the policy iteration algorithm (Cherrat et al., 2023).

A different approach to the maze or Gridworld problem is shown in (Dalla Pozza et al., 2022). Here, a classical RL agent is trained to modify the maze’s walls such as to maximize the escape probability with a quantum random walk in a given time interval.

3 Methods

3.1 Algorithm

Our hybrid learning agent uses, similar to (Hamann and Wölk, 2022), the variation of Grover’s algorithm where the number of solutions and thus the optimal number k_{opt} of amplitude amplification (AA) iterations is unknown (Boyer et al., 1998). This variation of the Grover algorithm appears also slightly varied as QSearch in (Brassard et al., 2002) and is necessary due to the fact that in a RL problem, the *success probability* of being rewarded is typically unknown.

The main ingredient of what we call from here on *Boyer’s algorithm* is a flexible interval $[0, m)$ with $m \in \mathbb{R}^+$, from which the integer number of AA iterations k is uniformly sampled. Starting from $m = 1$, the interval upper bound is multiplied by a constant factor $\lambda \in (1, 2)$ each time that the measurement yields no success. Once the parameter m reaches $\sqrt{1/p_{\text{min}}}$, with p_{min} being a lower bound for the current success probability, it is not increased further. At this point, Boyer’s algorithm reaches its so-called *critical stage*, at which the success probability in each AA round is known to be at least $1/4$, supposed that a rewarded item exists (Boyer et al., 1998).

Our learning algorithm (see Algorithm 1), is strongly intertwined with this notion of two stages in Boyer’s algorithm. The algorithm starts with a minimal episode length, which is $L = 1$ in the most uninformed case. We set the lower bound estimate

Algorithm 1 Probabilistic Hybrid Algorithm

Require: initial percept s_0 , set of actions \mathcal{A} , policy π , percept response function S , reward function R , Grover operator G

```

1:  $L \leftarrow 1$ 
2:  $m \leftarrow 1$ 
3:  $\lambda \leftarrow 5/4$ 
4:  $N_{\text{act}} = 0$  ▷ step counter
5: while true do
6:   ▷ probabilistic doubling of L ◁
7:    $q \leftarrow$  random number in  $[0, 1]$ 
8:   if  $q < \frac{2 \log(m)}{L \log(|\mathcal{A}|)}$  then
9:      $L \leftarrow 2 \cdot L$ 
10:     $m \leftarrow 1$ 
11:   ▷ amplitude amplification ◁
12:    $k \leftarrow$  random integer in  $[0, m]$ 
13:    $|\psi\rangle \leftarrow \sum_{\vec{a} \in \mathcal{A}^{\otimes L}} \sqrt{\pi(\vec{a})} |\vec{a}\rangle_A |\vec{s}_{\text{init}}\rangle_S |-\rangle_R$ 
14:    $|\psi'\rangle \leftarrow G^k |\psi\rangle$ 
15:    $\vec{a}' \leftarrow$  measure  $|\psi'\rangle$ 
16:    $N_{\text{act}} \leftarrow N_{\text{act}} + 2 \cdot k \cdot L$ 
17:   ▷ classical verification episode ◁
18:   for  $i = 1$  to  $L$  do
19:      $s_i \leftarrow S_i(s_{i-1}, a'_i)$ 
20:      $r_i \leftarrow R_i(s_{i-1}, a'_i)$ 
21:      $N_{\text{act}} \leftarrow N_{\text{act}} + 1$ 
22:     if  $r_i = 1$  then
23:        $\text{return } \vec{a}', N_{\text{act}}, (s_0, \dots, s_i), r_i$ 
24:   ▷ no reward ◁
25:    $m \leftarrow \min(\lambda \cdot m, \sqrt{|\mathcal{A}|^L})$ 

```

$p_{\min} = |\mathcal{A}|^{-L}$, assuming an uniform initial policy and at least one rewarded action sequence at the current episode length. In each round of the main loop, the episode length has a chance to be doubled, with probability

$$\varphi_L(m) \equiv \frac{\log(m)}{\log(\sqrt{|\mathcal{A}|^L})} = \frac{2 \log(m)}{L \log(|\mathcal{A}|)}. \quad (6)$$

This probability is chosen such that it reaches unity exactly when Boyer’s algorithm reaches its critical stage. If the episode length doubling is triggered, m is reset to one.

This probabilistic episode length selection strategy serves several purposes. First, starting from low episode length values is resource-friendly,

since the Hilbert space of action sequences, $\mathcal{H}_A^{\otimes L}$, scales exponentially with the episode length L . It is also more efficient with regard to the total number of actions played before reaching the target, which will be our main metric (see Section 4.1). Second, the exponential increase of L enables the hybrid algorithm to reach large episode lengths reasonably quickly, which might be necessary in scenarios with distant targets. Finally, coupling the doubling probability to the parameter m ensures that the algorithm does not spend too many tries with an episode length which has no, or vanishing, success chance.

3.2 Simulation

To systematically test our hybrid method, we focus on finding the first reward in a two-dimensional Gridworld scenario. The Gridworld layouts in our simulations have a quadratic *base area* without inner walls with one start and one target cell placed in diagonally opposing corners. In each cell, the RL agent may choose one action of the set $\mathcal{A} \in \{\text{up, down, left, right}\}$. The first action to reach the target cell in each episode yields a reward of one; every other action is not rewarded. Further, the quadratic base area is surrounded by outer walls. Standing next to a wall and choosing an action towards it yields no change in the cell state. Given that in the Gridworld sce-

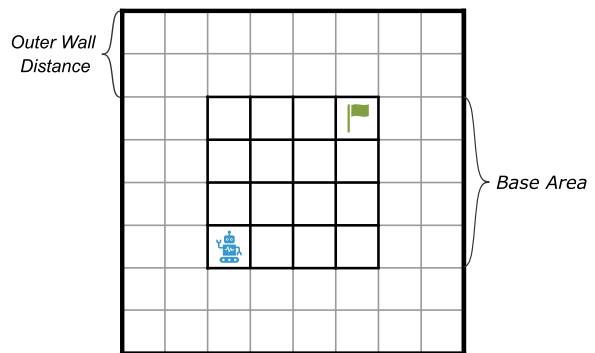


Fig. 2: Example of a Gridworld layout used in the simulations. The blue robot and the green flag symbols indicate the start and target position, respectively. The inner square of thick lines is the so-called *base area*, here with a size of 4×4 cells. The Gridworld has outer walls which prohibit the RL agent from moving away further. The example here shows an *outer wall distance* of 2.

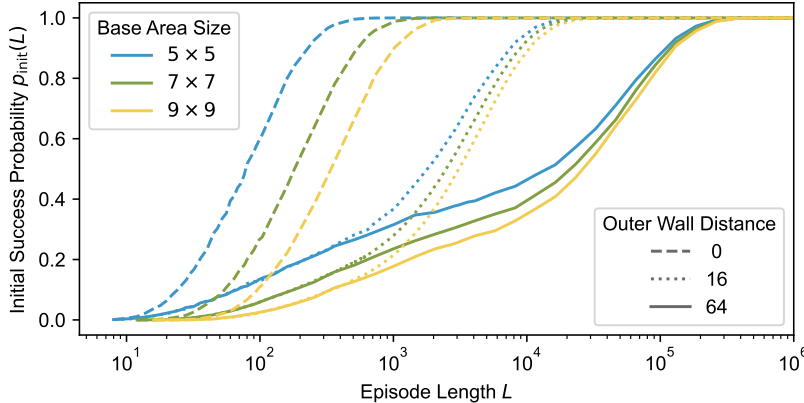


Fig. 3: Dependency of the agent’s initial success probability on its episode length L for different Gridworld layouts (varied by their base area size and outer wall distance). The probability values are generated using a Monte Carlo simulation, see Appendix B for more details.

nario, intermediate percepts of an episode depend on the actions played within that episode, the hybrid algorithm requires $\alpha_k = 2$ queries of the environment unitary U_{env} per iteration of the Grover operator G (cf. footnote 1 on page 4).

To generate a variety of shapes for the function $p_{\text{init}}(L)$ on which the performance of our strategies depends, we vary this basic Gridworld layout in two ways, as illustrated in Fig. 2:

1. We vary the side lengths of the quadratic base area, which we denote b . This obviously has an effect on the *minimal episode length* L_{min} necessary to reach the target, $L_{\text{min}} = 2(b - 1)$. Additionally, it influences the initial success probability for the minimal episode length (assuming a uniform policy initialization): $p_{\text{init}}(L_{\text{min}}) = \binom{2(b-1)}{b-1} \cdot 4^{-2(b-1)}$, with $\binom{2(b-1)}{b-1}$ being the number of distinct paths of length $2(b - 1) = L_{\text{min}}$ that reach the target.
2. We vary the distance of the outer walls around the Gridworld’s base area. An *outer wall distance*, or d_{wall} , of zero indicates that the walls are directly surrounding the base area. Having $d_{\text{wall}} = n$ would result in a ring of cells of thickness n between the base area and the outer walls. This has no effect on $p_{\text{init}}(L_{\text{min}})$. However, more distanced outer walls increase the general state space and, in particular, add cells to the state space which are further from the target cell than any cell in the Gridworld’s base area. Therefore, it effectively decreases how

quickly $p_{\text{init}}(L)$ rises with increasing episode length L .

In our simulations, we vary the Gridworld’s base area from size 5×5 (with $p_{\text{init}}(L_{\text{min}}) = 1.1 \times 10^{-3}$) to 9×9 ($p_{\text{init}}(L_{\text{min}}) = 2.9 \times 10^{-6}$). For the outer wall distance, we test the values 0, 4, 8, 16, 32, and 64. The scenario of no outer walls, which is equal to the limit of an infinite outer wall distance, is not computationally feasible to realize within our simulation framework (for an explanation and more implementation details, see Appendix B.) The dependency of $p_{\text{init}}(L)$ on a selection of the different Gridworld layouts is shown in Fig. 3.

Since we focus on the scenario of finding the first reward, we assume an untrained agent with an initial uniform policy $\pi(a) = \frac{1}{|\mathcal{A}|} \quad \forall a \in \mathcal{A}$. Every strategy is tested on each Gridworld layout for $N = 10\,000$ runs.

3.3 Classical Strategies

We compare the extended hybrid algorithm to two classical strategies, which we present and motivate in the following.

A direct classical equivalent to the extended hybrid algorithm can be devised by employing the same probabilistic episode length doubling strategy. Here, the parameter m of Algorithm 1 loses its twofold function and only defines the respective probability to double the episode length L .

This episode length then defines the number of steps the agent may take until it is reset to its starting position. From here on, we denote this the *probabilistic classical* strategy.

The second classical strategy arises from the idea that only in the hybrid algorithm an episode length needs to be given. Classical algorithms, however, are not restricted in such a way. Practically, not setting an episode length implies an uninterrupted random walk governed by the agent’s current policy until the reward state is reached. We denote this the *unrestricted classical* strategy.

4 Results

Before presenting the results of our simulation, we discuss the novel figure of merit and its implications. This figure of merit is different from the original hybrid learning agent introduced in (Hamann and Wölk, 2022).

4.1 Figure of Merit

The quadratic speedup that was proven theoretically and experimentally in the initial works on the hybrid learning agent (Hamann and Wölk, 2022; Saggio et al., 2021) is based on the number of queries of the environment unitary U_{env} . This is equivalent to the number of episodes played in a classical context.

This figure of merit is misleading in this scenario, as we now argue. Unlike in (Hamann and Wölk, 2022), we no longer operate with a fixed episode length in our RL scenario. Given that the episode length has a crucial impact on the agent’s initial success probability (cf. Fig. 3), omitting an episode’s length from the figure of merit is unreasonable in this scenario. Additionally, due to the monotonously increasing success probability, in the limit of an infinite episode length one singular episode is always sufficient to find the target.

Hence, we define the total number of actions taken, N_{act} , instead of the number of RL episodes as the new figure of merit in our scenario. With a current episode length of L , this metric is counted as follows:

- In the quantum part of the hybrid learning agent, k iterations of amplitude amplification add $2 \cdot k \cdot L$ steps to the count. Here, the factor two stems from the fact that we require $\alpha_k = 2$

applications of the environment unitary U_{env} per iteration of amplitude amplification.

- In the classical part of the hybrid learning agent and for a purely classical agent, an unsuccessful episode adds L steps to the count. If the agent reaches the target, only the actual number of steps $i \leq L$ necessary to reach the target is counted.

4.2 Simulation Results

A full overview of the results for each combination of strategy and Gridworld configuration is given in Table A1 of Appendix A. Fig. 4 visualizes the results on a subset of Gridworld configurations.

According to the two ways by which we varied the basic Gridworld layout, *base area size* b and *outer wall distance* d_{wall} , two effects can be observed in the data:

- The necessary number of actions to reach the target increases with increasing base area size b as expected. This observation holds for all strategies and outer wall distance values.
- The influence of the outer wall distance parameter, d_{wall} , differs for the different strategies. Thus, the question whether the hybrid agent or one of the classical agents is preferable depends on the outer wall distance.

At $d_{\text{wall}} = 0$ and $d_{\text{wall}} = 4$, the unrestricted classical agent requires on average the least number of actions to reach the target across all base area sizes. Both probabilistic strategies require approximately 1.2 to 5 times the number of actions, with the hybrid version requiring the most steps at larger base area sizes. For larger values of d_{wall} , both probabilistic strategies appear to stabilize in terms of N_{act} , which can be seen from the flat curves in Fig. 4 for outer wall distances of 8 and higher. Between the two, the hybrid strategy consistently has lower N_{act} , with the ratio of fewer actions ranging from 27% to 42% (for base area 9×9 with $d_{\text{wall}} = 8$ and base area 5×5 and $d_{\text{wall}} = 64$, respectively). For the unrestricted classical strategy, however, the number of actions increases continuously with increasing d_{wall} . At $d_{\text{wall}} = 8$, it is still more efficient than the hybrid agent for the two largest base area sizes, 8×8 and 9×9 . Already for $d_{\text{wall}} = 16$, however, it requires more actions than either probabilistic strategy for any base area size. For the largest

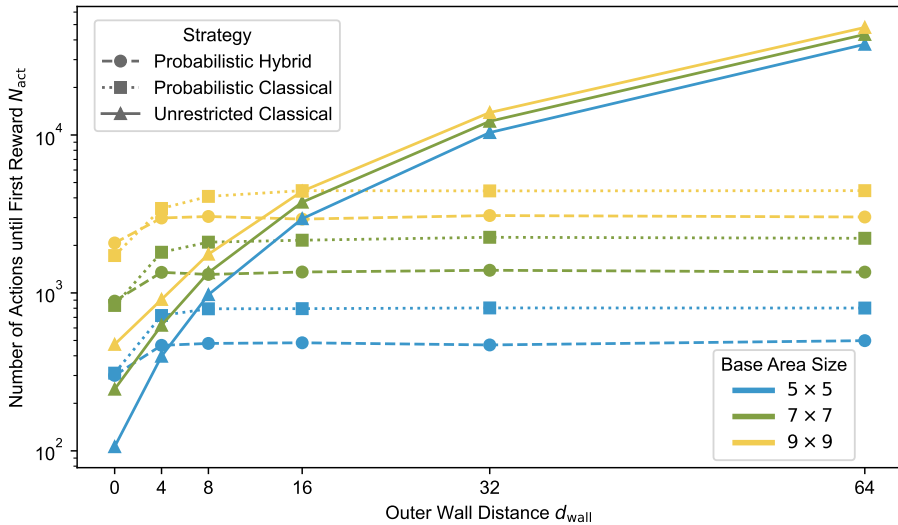


Fig. 4: Results of the tested hybrid and classical strategies for the first reward search problem. Gridworld layouts are varied by their base area size as well as their outer wall distance.

tested Gridworld configuration (base area size 9×9 and $d_{\text{wall}} = 64$), the unrestricted classical strategy trails the probabilistic hybrid one by more than an order of magnitude.

Another interesting quantity is the episode length at which the strategies terminate, coined *terminal episode length*. For the probabilistic strategies, this value is always a power of two due to the episode length doubling nature of the algorithms. A visual comparison of the relative frequencies with which either probabilistic strategy terminates at a specific episode length is given in Fig. 5. The probabilistic hybrid strategy terminates on average at lower episode lengths than the classical probabilistic strategy. For the Gridworld configuration used for Fig. 5 (base area 9×9 and $d_{\text{wall}} = 16$), the most frequent terminal episode lengths for the hybrid strategy are $2^5 = 32$ and $2^6 = 64$, whereas the probabilistic classical strategy terminates most frequently at $2^7 = 128$ and $2^8 = 256$. In Fig. 6, we compare the relative frequency of terminal episode lengths of the probabilistic hybrid algorithm with the total number of interaction steps that the original hybrid learning agent of (Hamann and Wölk, 2022) would require with a fixed episode length (cf. Fig. 1).

For the given Gridworld configuration, using the hybrid learning agent with fixed episode length

$L = 34$ would be optimal in terms of the total interaction steps. As the distribution of terminal episode lengths in Fig. 6 shows, our probabilistic hybrid algorithm terminates most frequently at the nearest ($L = 2^5 = 32$) and second most frequently at the second nearest ($L = 2^6 = 64$)

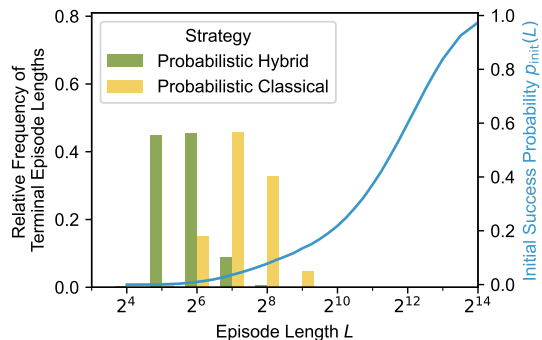


Fig. 5: Relative frequency of terminal episode lengths for the probabilistic hybrid and classical algorithms. The blue curve represents the initial success probability for the given Gridworld layout depending on the episode length. The results shown stem from the Gridworld configuration with a base area size of 9×9 and an outer wall distance of 16.

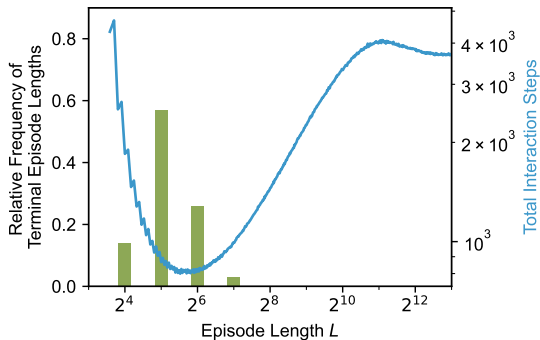


Fig. 6: Relative frequency of terminal episode lengths for the probabilistic hybrid algorithm and expected number of total interaction steps for the fixed-length hybrid algorithm (cf. Fig. 1). The Gridworld configuration used here has a base area size of 7×7 and an outer wall distance of 16.

episode length. This suggests that the in-built episode length doubling mechanism is tuned well enough that the probabilistic hybrid algorithm reaches efficient episode lengths and at the same time does not massively overshoot to unnecessary large episode lengths.

Fig. 7 shows the influence of the outer wall distance parameter on the terminal episode length. For the probabilistic hybrid strategy (Fig. 7a), increasing d_{wall} results in a slight shift of relative frequencies towards larger terminal episode lengths. Namely, the most frequent terminal episode length shifts from 32 for $d_{\text{wall}} = 0$ to 64 for $d_{\text{wall}} = 16$ and $d_{\text{wall}} = 64$. For the unrestricted classical strategy (Fig. 7b), the episode length shifts by several orders of magnitude for larger outer wall distances. As the figure shows, for $d_{\text{wall}} = 0$, it terminates most frequently at episode lengths between 2^8 and 2^9 , whereas for $d_{\text{wall}} = 16$ this interval ranges from 2^{12} to 2^{13} and for $d_{\text{wall}} = 64$ from 2^{15} to 2^{16} .

5 Conclusion

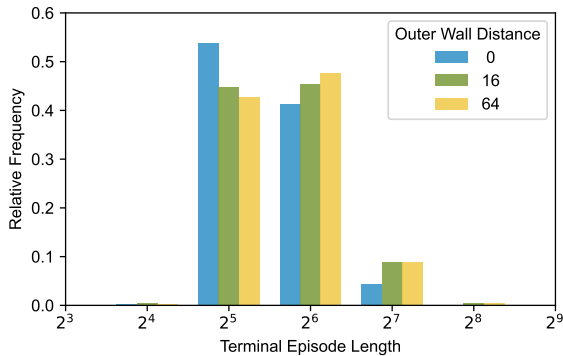
In this work, we have introduced a hybrid agent for quantum-accessible reinforcement learning with a flexible episode length selection strategy. As we have argued, this extension is crucial for finding the first reward in RL scenarios which are equivalent to a Gridworld with no information about the length of the shortest rewarded path.

The simulation results for different Gridworld configurations suggest that our proposed hybrid agent can (i) find the first reward faster and (ii) can find shorter solutions than the considered classical agents in many configurations.

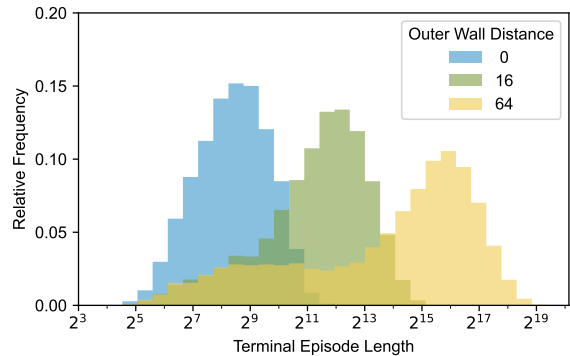
From the two options to vary the Gridworld layout, the outer wall distance proves to strongly influence which agent performs best. Whereas the unrestricted classical strategy requires more and more steps with increasing outer wall distance, the cost of the probabilistic strategies virtually remains the same after $d_{\text{wall}} \geq 8$. In the unrestricted classical case, the restricted state space from nearby walls helps the agent, since it can effectively never distance itself further from the target than it is from the starting position. With an increasing outer wall distance, however, the agent may very well initially move in a wrong direction and thus effectively increase its distance from the target. Here, resetting the agent to its starting position is beneficial, which is exactly what the probabilistic strategies do due to their finite episode length. Given that the probabilistic strategies terminate at much lower episode lengths than the unrestricted classical strategy (cf. Figs. 5 and 7), they are hardly affected by the ever increasing state space, as the flat curves in Fig. 4 indicate.

Between the two probabilistic strategies, the hybrid one proves to find the target quicker in all layouts except the most trivial one with $d_{\text{wall}} = 0$. Whereas the quadratic scaling advantage does not apply any more for this metric and scenario, the hybrid strategy outperforms its classical counterpart in many cases. Especially towards lower initial success probabilities and larger state spaces, i.e., harder problems, the hybrid agent’s amplitude amplification appears to be advantageous.

The effect of increasing the Gridworld’s base area size is the same for all agents: it makes the problem harder overall. Comparing the distributions of terminal episode lengths of the different strategies and the initial success probability curve $p_{\text{init}}(L)$ in Fig. 5 also reveals that the doubling of the episode length happens slow enough such that (i) the maximal episode length stays in a reasonable regime and that (ii) noticeable speedups through amplitude amplification can be achieved. In addition, the lower terminal episode length suggests that the solutions found by the hybrid agent are shorter on average than the ones found



(a) Probabilistic hybrid strategy.



(b) Unrestricted classical strategy.

Fig. 7: Comparison of the terminal episode lengths between the probabilistic hybrid and the unrestricted classical strategy. The results shown are for the configuration with a base area size of 9×9 .

by the probabilistic classical strategy. This can lead to additional advantages in the further learning resulting in, e.g., faster or better learning results. Further, the comparison with our motivating example in Fig. 6 suggests that even without prior knowledge of the optimal episode length, the probabilistic hybrid algorithm terminates most frequently at the episode lengths closest to it.

Finally, we address a few design questions on the chosen Gridworld layout, especially regarding a few omissions of further Gridworld variations. First, one could conceive of a scenario where moving into some cells, or even all walls, stops the episode immediately without a reward. If we have a move sequence \vec{a} which moves into such a terminal, but non-rewarded cell, concatenating any additional move sequence \vec{a}' will not turn the full sequence into a rewarded one. Thus, with our initial uniform policy, the initial success probability does not converge to 1 in the limit of infinite episode lengths. Here, it can be assumed that the probabilistic hybrid strategy is beneficial as this strategy works well with a slowly increasing success probability and low probabilities in general. Second, one could omit the outer walls altogether, yielding an infinite state space. As mentioned in Section 3.2, simulating this scenario is not feasible. However, we can extrapolate the trend for increasing outer wall distances, since having no outer walls is equal to the limit $d_{\text{wall}} \rightarrow \infty$. Here, we can see that the probabilistic strategies prove to be advantageous, with the hybrid version still

requiring less steps than the classical one. Third and last, one could investigate higher-dimensional Gridworld layouts than the two-dimensional scenario shown here. For random walks in hypergrids of dimension $D \geq 3$, however, the probability to reach any point with a random walk in the limit of infinite steps does not converge to unity (Pólya, 1921). Therefore, an infinite random walk in the fashion of the unrestricted classical strategy is certainly a bad choice. Given that, besides the asymptotic limit, the scenario is not fundamentally different, the hybrid probabilistic strategy can again be assumed to be the most efficient of the three, supposed that the initial success probability is low.

There are two research questions which should be investigated further: (i) Is the coincidence of the most probable terminal episode length with the optimal episode length pure luck or a reliable property of our algorithm? (ii) In which ways does the on average shorter terminal episode length of our probabilistic hybrid agent compared to the probabilistic classical agent influence the further learning? In addition, the successful extension of the hybrid learning agent to episodic learning tasks with unknown target distance now enables the application to many more realistic learning tasks, which should be investigated in the future.

Acknowledgements. This project was made possible by the DLR Quantum Computing Initiative and the Federal Ministry for Economic Affairs and Climate Action;

qci.dlr.de/projects/qlearning. The authors gratefully acknowledge the scientific support and HPC resources provided by the German Aerospace Center (DLR). The HPC system CARA is partially funded by “Saxon State Ministry for Economic Affairs, Labour and Transport” and “Federal Ministry for Economic Affairs and Climate Action”. The authors thank Alessio Belenchia and Benjamin Desef for helpful comments.

Declarations

Competing interests. The authors declare no competing interests.

References

- Biamonte, J., Bergholm, V.: Tensor Networks in a Nutshell (2017). <https://arxiv.org/abs/1708.00006>
- Biamonte, J., Wittek, P., Pancotti, N., Rebentrost, P., Wiebe, N., Lloyd, S.: Quantum machine learning. *Nature* **549**(7671), 195–202 (2017) <https://doi.org/10.1038/nature23474>
- Boyer, M., Brassard, G., Høyer, P., Tapp, A.: Tight bounds on quantum searching. *Fortschr. Phys.* **46**(4-5), 493–505 (1998) [https://doi.org/10.1002/\(SICI\)1521-3978\(199806\)46:4/5<493::AID-PROP493>3.0.CO;2-P](https://doi.org/10.1002/(SICI)1521-3978(199806)46:4/5<493::AID-PROP493>3.0.CO;2-P)
- Brassard, G., Høyer, P., Mosca, M., Tapp, A.: Quantum amplitude amplification and estimation. *Contemp. Math.* **305**, 53–74 (2002) <https://doi.org/10.1090/conm/305/05215>
- Bridgeman, J.C., Chubb, C.T.: Hand-waving and interpretive dance: an introductory course on tensor networks. *J. Phys. A* **50**(22), 223001 (2017) <https://doi.org/10.1088/1751-8121/aa6dc3>
- Briegel, H.J., Cuevas, G.: Projective simulation for artificial intelligence. *Sci. Rep.* **2**(1), 400 (2012) <https://doi.org/10.1038/srep00400>
- Brockman, G., Cheung, V., Pettersson, L., Schneider, J., Schulman, J., Tang, J., Zaremba, W.: OpenAI Gym (2016). <https://arxiv.org/abs/1606.01540>
- Bukov, M., Day, A.G.R., Sels, D., Weinberg, P., Polkovnikov, A., Mehta, P.: Reinforcement learning in different phases of quantum control. *Phys. Rev. X* **8**, 031086 (2018) <https://doi.org/10.1103/PhysRevX.8.031086>
- Cerezo, M., Arrasmith, A., Babbush, R., Benjamin, S.C., Endo, S., Fujii, K., McClean, J.R., Mitarai, K., Yuan, X., Cincio, L., Coles, P.J.: Variational quantum algorithms. *Nat. Rev. Phys.* **3**(9), 625–644 (2021) <https://doi.org/10.1038/s42254-021-00348-9>
- Cerezo, M., Larocca, M., García-Martín, D., Diaz, N.L., Braccia, P., Fontana, E., Rudolph, M.S., Bermejo, P., Ijaz, A., Thanasilp, S., Anschuetz, E.R., Holmes, Z.: Does provable absence of barren plateaus imply classical simulability? Or, why we need to rethink variational quantum computing (2024). <https://arxiv.org/abs/2312.09121>
- Chen, S.Y.-C., Yang, C.-H.H., Qi, J., Chen, P.-Y., Ma, X., Goan, H.-S.: Variational quantum circuits for deep reinforcement learning. *IEEE Access* **8**, 141007–141024 (2020) <https://doi.org/10.1109/ACCESS.2020.3010470>
- Chen, H.-Y., Chang, Y.-J., Liao, S.-W., Chang, C.-R.: Deep q-learning with hybrid quantum neural network on solving maze problems. *Quantum Mach. Intell.* **6**(1), 2 (2024) <https://doi.org/10.1007/s42484-023-00137-w>
- Cherrat, E.A., Kerenidis, I., Prakash, A.: Quantum reinforcement learning via policy iteration. *Quantum Mach. Intell.* **5**(2), 30 (2023) <https://doi.org/10.1007/s42484-023-00116-1>
- Dalla Pozza, N., Buffoni, L., Martina, S., Caruso, F.: Quantum reinforcement learning: the maze problem. *Quant. Mach. Intell.* **4**(1), 11 (2022) <https://doi.org/10.1007/s42484-022-00068-y>
- Dong, D., Chen, C., Li, H., Tarn, T.-J.: Quantum reinforcement learning. *IEEE Trans. Syst. Man. Cybern. B Cybern.* **38**(5), 1207–1220 (2008) <https://doi.org/10.1109/TSMCB.2008.925743>
- Dunjko, V., Taylor, J.M., Briegel, H.J.: Quantum-enhanced machine learning. *Phys. Rev. Lett.* **117**, 130501 (2016) <https://doi.org/10.1103/>

- PhysRevLett.117.130501
- Fösel, T., Tighineanu, P., Weiss, T., Marquardt, F.: Reinforcement learning with neural networks for quantum feedback. *Phys. Rev. X* **8**, 031084 (2018) <https://doi.org/10.1103/PhysRevX.8.031084>
- Fösel, T., Niu, M.Y., Marquardt, F., Li, L.: Quantum circuit optimization with deep reinforcement learning (2021). <https://arxiv.org/abs/2103.07585>
- Ganguly, B., Wu, Y., Wang, D., Aggarwal, V., Ganguly, B., Wu, Y., Wang, D., Aggarwal, V.: Quantum Computing Provides Exponential Regret Improvement in Episodic Reinforcement Learning (2023). <https://arxiv.org/abs/2302.08617>
- Grover, L.K.: Quantum mechanics helps in searching for a needle in a haystack. *Phys. Rev. Lett.* **79**, 325–328 (1997) <https://doi.org/10.1103/PhysRevLett.79.325>
- Guatto, M., Susto, G.A., Ticozzi, F.: Improving robustness of quantum feedback control with reinforcement learning. *Phys. Rev. A* **110**, 012605 (2024) <https://doi.org/10.1103/PhysRevA.110.012605>
- Hamann, A., Dunjko, V., Wölk, S.: Quantum-accessible reinforcement learning beyond strictly epochal environments. *Quantum Mach. Intell.* **3**(2), 22 (2021) <https://doi.org/10.1007/s42484-021-00049-7>
- Hamann, A., Wölk, S.: Performance analysis of a hybrid agent for quantum-accessible reinforcement learning. *New J. Phys.* **24**(3), 033044 (2022) <https://doi.org/10.1088/1367-2630/ac5b56>
- Hohenfeld, H., Heimann, D., Wiebe, F., Kirchner, F.: Quantum deep reinforcement learning for robot navigation tasks. *IEEE Access* **12**, 87217–87236 (2024) <https://doi.org/10.1109/ACCESS.2024.3417808>
- Huggins, W., Patil, P., Mitchell, B., Whaley, K.B., Stoudenmire, E.M.: Towards quantum machine learning with tensor networks. *Quantum Sci. Technol.* **4**(2), 024001 (2019) <https://doi.org/10.1088/2058-9565/aaea94>
- Jerbi, S., Gyurik, C., Marshall, S.C., Briegel, H.J., Dunjko, V.: Parametrized quantum policies for reinforcement learning. In: *Advances in Neural Information Processing Systems 34: Annual Conference on Neural Information Processing Systems 2021, NeurIPS 2021, Virtual event*, pp. 28362–28375 (2021). <https://proceedings.neurips.cc/paper/2021/hash/eec96a7f788e88184c0e713456026f3f-Abstract.html>
- Kitaev, A.Y.: Quantum measurements and the Abelian Stabilizer Problem (1995). <https://arxiv.org/abs/quant-ph/9511026>
- Kwiatkowski, A., Towers, M., Terry, J., Balis, J.U., De Cola, G., Deleu, T., Goulão, M., Kallinteris, A., Krimmel, M., KG, A., Perez-Vicente, R., Pierré, A., Schulhoff, S., Tai, J.J., Tan, H., Younis, O.G.: Gymnasium: A Standard Interface for Reinforcement Learning Environments (2024). <https://arxiv.org/abs/2407.17032>
- Lillicrap, T.P., Hunt, J.J., Pritzel, A., Heess, N., Erez, T., Tassa, Y., Silver, D., Wierstra, D.: Continuous control with deep reinforcement learning (2019). <https://arxiv.org/abs/1509.02971>
- Lockwood, O.: Optimizing Quantum Variational Circuits with Deep Reinforcement Learning (2022). <https://arxiv.org/abs/2109.03188>
- Lockwood, O., Si, M.: Reinforcement learning with quantum variational circuits. In: *Proceedings of the AAAI Conference on Artificial Intelligence and Interactive Digital Entertainment*, Lexington, KY (2020). <https://doi.org/10.1609/aiide.v16i1.7437>
- Lockwood, O., Si, M.: Playing atari with hybrid quantum-classical reinforcement learning. In: *NeurIPS 2020 Workshop on Pre-registration in Machine Learning*, Virtual event (2021). <http://proceedings.mlr.press/v148/lockwood21a.html>
- Mnih, V., Kavukcuoglu, K., Silver, D., Rusu, A.A., Veness, J., Bellemare, M.G., Graves,

- A., Riedmiller, M., Fidjeland, A.K., Ostrovski, G., Petersen, S., Beattie, C., Sadik, A., Antonoglou, I., King, H., Kumaran, D., Wierstra, D., Legg, S., Hassabis, D.: Human-level control through deep reinforcement learning. *Nature* **518**(7540), 529–533 (2015) <https://doi.org/10.1038/nature14236>
- Nautrup, H.P., Delfosse, N., Dunjko, V., Briegel, H.J., Friis, N.: Optimizing Quantum Error Correction Codes with Reinforcement Learning. *Quantum* **3**, 215 (2019) <https://doi.org/10.22331/q-2019-12-16-215>
- Nielsen, M.A., Chuang, I.L.: *Quantum Computation and Quantum Information: 10th Anniversary Edition*. Camb. Univ. Press, Cambridge (2010). <https://doi.org/10.1017/CBO9780511976667>
- Orús, R.: A practical introduction to tensor networks: Matrix product states and projected entangled pair states. *Ann. Phys.* **349**, 117–158 (2014) <https://doi.org/10.1016/j.aop.2014.06.013>
- Ostaszewski, M., Trenkwalder, L.M., Masarczyk, W., Scerri, E., Dunjko, V.: Reinforcement learning for optimization of variational quantum circuit architectures. In: *Advances in Neural Information Processing Systems 34: Annual Conference on Neural Information Processing Systems 2021, NeurIPS 2021, Virtual event*, pp. 18182–18194 (2021). <https://proceedings.neurips.cc/paper/2021/hash/9724412729185d53a2e3e7f889d9f057-Abstract.html>
- Paparo, G.D., Dunjko, V., Makmal, A., Martin-Delgado, M.A., Briegel, H.J.: Quantum speedup for active learning agents. *Phys. Rev. X* **4**, 031002 (2014) <https://doi.org/10.1103/PhysRevX.4.031002>
- Pólya, G.: Über eine Aufgabe der Wahrscheinlichkeitsrechnung betreffend die Irrfahrt im Straßennetz. *Math. Ann.* **84**(1), 149–160 (1921) <https://doi.org/10.1007/BF01458701>
- Preskill, J.: Quantum Computing in the NISQ era and beyond. *Quantum* **2**, 79 (2018) <https://doi.org/10.22331/q-2018-08-06-79>
- Rapp, F., Kreplin, D.A., Huber, M.F., Roth, M.: Reinforcement learning-based architecture search for quantum machine learning (2024). <https://arxiv.org/abs/2406.02717>
- Ruiz, F.J.R., Laakkonen, T., Bausch, J., Balog, M., Barekatin, M., Heras, F.J.H., Novikov, A., Fitzpatrick, N., Romera-Paredes, B., Wetering, J., Fawzi, A., Meichanetzidis, K., Kohli, P.: Quantum Circuit Optimization with AlphaTensor (2024). <https://arxiv.org/abs/2402.14396>
- Saggio, V., Asenbeck, B.E., Hamann, A., Strömberg, T., Schiansky, P., Dunjko, V., Friis, N., Harris, N.C., Hochberg, M., Englund, D., Wölk, S., Briegel, H.J., Walther, P.: Experimental quantum speed-up in reinforcement learning agents. *Nature* **591**(7849), 229–233 (2021) <https://doi.org/10.1038/s41586-021-03242-7>
- Schuld, M., Killoran, N.: Is quantum advantage the right goal for quantum machine learning? *PRX Quantum* **3**, 030101 (2022) <https://doi.org/10.1103/PRXQuantum.3.030101>
- Schulman, J., Wolski, F., Dhariwal, P., Radford, A., Klimov, O.: Proximal Policy Optimization Algorithms (2017). <https://arxiv.org/abs/1707.06347>
- Silver, D., Lever, G., Heess, N., Degris, T., Wierstra, D., Riedmiller, M.: Deterministic policy gradient algorithms. In: *Proceedings of the 31st International Conference on Machine Learning, Beijing, China*, pp. 387–395 (2014). <https://proceedings.mlr.press/v32/silver14.html>
- Silver, D., Schrittwieser, J., Simonyan, K., Antonoglou, I., Huang, A., Guez, A., Hubert, T., Baker, L., Lai, M., Bolton, A., Chen, Y., Lillicrap, T., Hui, F., Sifre, L., Driessche, G., Graepel, T., Hassabis, D.: Mastering the game of go without human knowledge. *Nature* **550**(7676), 354–359 (2017) <https://doi.org/10.1038/nature24270>
- Sivak, V.V., Eickbusch, A., Liu, H., Royer, B., Tsioutsios, I., Devoret, M.H.: Model-free quantum control with reinforcement learning. *Phys. Rev. X* **12**, 011059 (2022) <https://doi.org/10.1103/PhysRevX.12.011059>

- Sivak, V.V., Eickbusch, A., Royer, B., Singh, S., Tsioutsios, I., Ganjam, S., Miano, A., Brock, B.L., Ding, A.Z., Frunzio, L., Girvin, S.M., Schoelkopf, R.J., Devoret, M.H.: Real-time quantum error correction beyond break-even. *Nature* **616**(7955), 50–55 (2023) <https://doi.org/10.1038/s41586-023-05782-6>
- Skolik, A., Jerbi, S., Dunjko, V.: Quantum agents in the Gym: a variational quantum algorithm for deep Q-learning. *Quantum* **6**, 720 (2022) <https://doi.org/10.22331/q-2022-05-24-720>
- Sriarunothai, T., Wölk, S., Giri, G.S., Friis, N., Dunjko, V., Briegel, H.J., Wunderlich, C.: Speeding-up the decision making of a learning agent using an ion trap quantum processor. *Quantum Sci. Technol.* **4**(1), 015014 (2018) <https://doi.org/10.1088/2058-9565/aaef5e>
- Sutton, R.S., Barto, A.G.: Reinforcement Learning: An Introduction. 2nd Edition. A Bradford Book, Cambridge (2018). <http://incompleteideas.net/book/the-book-2nd.html>
- Watkins, C.J.C.H., Dayan, P.: Q-learning. *Mach. Learn.* **8**(3), 279–292 (1992) <https://doi.org/10.1007/BF00992698>
- Wiedemann, S., Hein, D., Udluft, S., Mendl, C.: Quantum Policy Iteration via Amplitude Estimation and Grover Search – Towards Quantum Advantage for Reinforcement Learning (2023). <https://arxiv.org/abs/2206.04741>
- Zhong, H., Hu, J., Xue, Y., Li, T., Wang, L.: Provably Efficient Exploration in Quantum Reinforcement Learning with Logarithmic Worst-Case Regret (2024). <https://arxiv.org/abs/2302.10796>

Appendix A Table of Full Results

Table A1: Results of the tested hybrid and classical strategies for the first reward search problem. Numbers represent average N_{act} (with the respective standard error in parentheses) for the different Gridworld layouts, based on $N = 10\,000$ runs per configuration. For each configuration, the lowest value of N_{act} is printed in boldface.

Outer Wall Distance	Strategy	Base Area Size				
		5×5	6×6	7×7	8×8	9×9
0	Probabilistic Hybrid	300(2)	515(3)	887(5)	1400(9)	2071(14)
	Probabilistic Classical	310(2)	534(3)	833(5)	1208(7)	1724(9)
	Unrestricted Classical	106(1)	170(2)	246(2)	347(3)	472(4)
4	Probabilistic Hybrid	466(3)	806(4)	1350(7)	2087(11)	2981(17)
	Probabilistic Classical	720(6)	1206(9)	1809(12)	2541(16)	3426(21)
	Unrestricted Classical	397(4)	503(5)	624(6)	749(7)	909(8)
8	Probabilistic Hybrid	479(3)	797(5)	1309(8)	2106(14)	3048(18)
	Probabilistic Classical	793(7)	1333(11)	2096(16)	3083(23)	4085(29)
	Unrestricted Classical	975(10)	1165(11)	1343(13)	1539(14)	1758(16)
16	Probabilistic Hybrid	483(3)	826(4)	1357(7)	1986(11)	2934(17)
	Probabilistic Classical	795(7)	1374(12)	2157(18)	3115(24)	4442(34)
	Unrestricted Classical	2950(34)	3375(37)	3754(41)	4095(43)	4406(45)
32	Probabilistic Hybrid	468(3)	816(5)	1391(8)	2047(12)	3090(18)
	Probabilistic Classical	803(7)	1364(12)	2250(18)	3291(26)	4426(34)
	Unrestricted Classical	10 357(135)	11 219(139)	12 208(151)	13 152(154)	13 872(157)
64	Probabilistic Hybrid	499(3)	847(5)	1355(7)	2173(12)	3025(18)
	Probabilistic Classical	802(7)	1385(12)	2218(18)	3147(25)	4442(34)
	Unrestricted Classical	37 514(543)	40 668(555)	43 315(578)	46 448(606)	47 963(615)

Appendix B Simulation Details

Given that amplitude amplification (AA) is not a NISQ-compatible algorithm, we have to fall back to simulating its effect instead of doing a full quantum circuit execution on simulated or real hardware.

To do so, we infer the initial success probability $p_{\text{init}}(L)$ for any episode length L which might occur in the hybrid strategy beforehand. Having knowledge of this probability, we can subsequently compute the amplified success probability using the well-known AA equation (Brassard et al., 2002)

$$p_{AA}(L, k) = \sin^2 \left([2k + 1] \arcsin \left[p_{\text{init}}(L)^{-1/2} \right] \right)$$

for k iterations of our Grover operator G . This probability can in turn be used to correctly sample a rewarded or non-rewarded action sequence.

Given that the initial policy which generates $p_{\text{init}}(L)$ is a uniform probability distribution over the space of actions, the agent’s movement initially equals an unweighted random walk. Therefore, we can estimate $p_{\text{init}}(L)$ with a Monte Carlo simulation of random walks of length L .

For each combination of Gridworld configuration and episode length L to be tested, we perform at least $N_{\text{shots}}(L) = 2^{14}$ runs and count the number of random walks which terminated successfully, $N_{\text{success}}(L)$ (i.e., which have the target cell in their path). To improve numerical stability, we keep incrementing $N_{\text{shots}}(L)$ in batches of 2^{14} until $N_{\text{success}}(L)$ has reached at least 16. Doing so, we can finally estimate the initial success probability simply as the ratio of successes to shots:

$$p_{\text{init}}(L) \approx \frac{N_{\text{success}}(L)}{N_{\text{shots}}(L)}.$$

Due to the hybrid agent’s doubling strategy, $p_{\text{init}}(L)$ only needs to be pre-computed for powers of 2 and until convergence of $p_{\text{init}}(L)$. For the plot in Fig. 3, however, we also computed $p_{\text{init}}(L)$ for intermediate values to create a smoother curve using linear interpolation.

Finally, in this section we address why omitting outer walls at all is not feasible within this

framework. As proven in (Pólya, 1921), on an infinite two-dimensional grid, the random walker’s probability to pass by any given point $\mathbf{x} \in \mathbb{Z}^2$ converges to 1 in the limit of infinite steps. Therefore, even for the scenario of no walls, which is equivalent to an infinite two-dimensional grid, $p_{\text{init}}(L)$ should converge towards one in the limit of infinite steps,

$$\lim_{L \rightarrow \infty} p_{\text{init}}(L) = 1.$$

The issue for our simulation is, however, the slow rate of convergence. Even for the smallest base area size of 5×5 , $p_{\text{init}}(L)$ has just reached approximately 60% for $L = 2^{22} = 4\,194\,304$ in the “no-walls” scenario, whereas for $d_{\text{wall}} = 64$ the probability already converges near $L = 2^{19} = 1\,048\,576$. By counting just the steps of unsuccessful random walks, we thus arrive at

$$\begin{aligned} & L \cdot (1 - p_{\text{init}}(L)) \cdot N_{\text{shots}} \\ & \approx 2^{22} \cdot (1 - 0.6) \cdot 2^{14} \\ & \approx 2.7 \times 10^{10} \end{aligned}$$

steps computed just for this episode length, which becomes soon fully intractable for even larger episode lengths due to the slow increase in $p_{\text{init}}(L)$.

Additionally, the run time scaling of the unrestricted classical strategy in Fig. 4 with increasing outer wall distance shows the intractability of simulating this strategy in a “no-walls” scenario.

Appendix C Total Interaction Steps for Fixed Episode Length

In this section, we give some background on the performance comparison shown in Fig. 1, which motivates the flexible episode length selection strategy for the hybrid agent.

The example stems from an RL setting of a Gridworld with a base area size of 7×7 and an outer wall distance of 16 (see Section 3.2 for our Gridworld layout definitions). We choose fixed episode lengths L in the interval ranging from $L_{\text{min}} = 12$ up to $2^{14} = 16\,384$. Further, we assume untrained agents initialized with uniform action selection probabilities such that the classical success probability $p_{\text{init}}(L)$ is the one of a random walk of length L through the maze. For both

the classical and hybrid agent, we count the total number of interaction steps, i.e., the total number of actions performed until the first reward is reached.

The results presented in Fig. 1 are generated with a Monte Carlo simulation of 100 000 repetitions each on a logarithmically-spaced grid of 868 different episode length values. For the classical agent, we perform a random walk that is periodically reset after L steps until the first reward is found, aggregating the total number of steps. For the hybrid agent, we rely on the simulation of amplitude amplification presented in Appendix B, using the precomputed initial success probabilities for each episode length. If the simulated amplitude amplification returns a rewarded episode, we sample the length of a rewarded action sequence by performing random walks of at most length L until there is a rewarded one.

The “zig-zag” behavior in Fig. 1 for small episode lengths can be explained as follows. For the chosen Gridworld layout, the minimal episode length to reach the target is twelve. As we increase the episode length, non-optimal paths may now also reach the target, resulting in an increase of the success probability. However, this increase only occurs in episode length intervals of two as one cannot land on the target cell with an odd number of steps. Thus, for small episode lengths, the success probability only increases from an even number to the next but stays constant for the next larger odd value. Only when the episode length is large enough that the agent may run into a wall and thus “waste” a step, the success probability increases for every incrementally larger episode length. This piecewise constant success probability leads to the spikes for odd episode length values in Fig. 1. Indeed, there are on average as many unsuccessful episodes as with the next lower even episode length, but these episodes are more “costly” due to the additional step.